J Bio Tribo Corros (2017) 3:39
DOI 10.1007/s40735-017-0100-5

Corrosion and Wear Properties of Ti/Tetrahedral Amorphous Carbon Multilayered Coating

S. Viswanathan[1] · M. Manjunath Reddy[1] · L. Mohan[1] · Parthasarathi Bera[1] · Harish C. Barshilia[1] · C. Anandan[1]

Received: 30 April 2017 / Revised: 28 June 2017 / Accepted: 3 July 2017 / Published online: 13 July 2017
© Springer International Publishing AG 2017

Abstract The titanium and tetrahedral amorphous carbon (Ti/ta-C) multilayered coating has been deposited by combination of cathodic arc evaporation and magnetron sputtering employing graphite and titanium targets with constant substrate bias voltage of −110 V. Coating has been developed with titanium and tetrahedral amorphous carbon alternatively on silicon and stainless steel 202 substrates with total thickness of 936 nm. The coating has been characterized by field emission scanning electron microscopy, energy-dispersive spectroscopy, atomic force microscopy, Raman spectroscopy and X-ray photoelectron spectroscopy. Coating properties have been investigated by nanoindentation, potentiodynamic polarization and reciprocating wear studies. Observed average hardness values of the multilayered coating are 15.6 ± 1.7 and 17 ± 3.6 GPa at 1 and 2 mN loads, respectively. The Ti/ta-C multilayered coating exhibits enhanced corrosion resistance with better passive behavior in 3.5% NaCl solution, and corrosion potential is observed to move more positive values. The reciprocating wear studies demonstrate very low coefficient of friction of 0.07−0.2 at 2, 5, 7 and 10 N loads.

Keywords Ti/ta-C multilayer · XPS · Corrosion · EIS · Wear

✉ Parthasarathi Bera
partho@nal.res.in

✉ C. Anandan
canandan@yahoo.com

[1] Surface Engineering Division, CSIR-National Aerospace Laboratories, Bengaluru 560017, India

1 Introduction

Hydrogen-free amorphous carbon generally called as a tetrahedral amorphous carbon (ta-C) contains high fraction of sp^3 content, and this carbon is known as hydrogenated amorphous carbon (ta-C:H) when it is hydrogenated [1, 2]. The ta-C and ta-C:H have been used as coating materials and show interesting properties such as high hardness, chemical inertness and wear resistance because of high sp^3 content [1–5] leading to its wide range of applications including optical, mechanical and electronics [6–8]. Their beneficial properties arise from sp^3 content of their bonding, and these carbons are frequently called diamond-like carbon (DLC). This coating has widely been prepared by filtered cathodic vacuum arc techniques for industrial and laboratory scale. It provides highly ionized plasma and high deposition rate of high tetrahedrally bonded amorphous carbon coating [9–13]. However, high residual stress in amorphous carbon limits the coating thickness which leads to poor adhesion to the substrate, resulting in the peeling off of the coating or delaminating. These problems can be overcome by metal incorporation into the coating and multilayered coating [14, 15]. It has also been found that incorporation of metals in amorphous carbon is one of the effective ways to enhance its mechanical and tribological properties. Recently, numerous metal dopants such as Ti, Mo, W, Si, Cr and Al have been used to enhance the properties of the ta-C coatings [16, 17]. Among these dopant elements, Ti has much attention in industrial and laboratory sectors because of the good adhesion with all substrates and easy reaction with carbon [18]. Ti-incorporated carbon surface acts as a diffusion barrier for impeding the diffusion of oxygen into the sublayer [19], thus preventing the incursion and destruction of oxygen to the crosslinked carbon network. Titanium-incorporated DLC

coatings have extensively been studied by many researchers. Zhao et al., Cui et al. and Qiang et al. have demonstrated that diamond-like carbon coatings with different concentrations of titanium show superior tribological performance [20–22]. However, higher concentration of titanium leads to break up the continuity of the carbon network in coating resulting in lower hardness [23–25].

Several techniques are available to deposit amorphous carbon coatings such as filtered cathodic vacuum arc (FCVA) [24–26], filtered pulsed arc discharge (FPAD) [27], sputtering deposition [28], plasma-enhanced chemical vapor deposition (PECVD) [29–31], metal vapor vacuum arc (MeVVA) [32–34] and plasma source ion implantation (PSII) [35]. In this study, Ti/ta-C multilayered coating has been deposited by combination of unfiltered cathodic arc evaporation and magnetron sputtering. The coating has been characterized by FESEM, EDS, AFM, Raman spectroscopy and XPS. Corrosion and wear behaviors of the coating have also been investigated.

2 Materials and Methods

2.1 Preparation of Substrates

In the present work, silicon wafers (100) and glass slides were cut into appropriate sizes and cleaned in acetone ultrasonically. These samples were used for thickness measurement, nanohardness testing, Raman spectroscopy and XPS studies. Stainless steel (SS) 202 sheets were cut into 2.5 × 2.5 cm^2 pieces, and they were ground by different grit sized silicon carbide emery papers to smoothen the surface and then polished by 0.3 μm alumina powder mixed with distilled water to get mirror-like finish. The polished stainless steel samples were then ultrasonically cleaned for 20 min in acetone and then loaded in the vacuum chamber for coating deposition. These samples were used for corrosion and wear studies.

2.2 Deposition of Ti/ta-C Multilayered Coating

Ti/ta-C multilayered coating was deposited with combination of cathodic arc evaporation and magnetron sputtering. The deposition chamber was made of stainless steel. The chamber was evacuated to base vacuum of 5.7 × 10^{-6} mbar by a turbomolecular pump backed by a rotary pump. After the base pressure was reached, the chamber and gas lines were purged with argon and hydrogen gas. These gases were introduced into the chamber by a showerhead-type distributor, and flow rates were controlled by mass flow controllers (MSK Instruments, USA) and a throttle valve. Prior to deposition, the surfaces of the silicon and stainless steel (SS 202) substrates were etched with hydrogen plasma for 20 min with substrate bias of −110 V. Ti deposition over ta-C coating was carried out in the same vacuum system. The vacuum chamber consists of magnetron sputtering head with titanium target of 3 in. diameter and 6 mm thickness. A graphite target of 3 in. diameter was used for cathodic arc evaporation (CAE) for the deposition of tetrahedral amorphous carbon coating. Magnetron sputtering and CAE were employed alternatively to deposit multilayered coatings consisting of Ti and ta-C layers. Sputter deposition was carried by 10 sscm of Ar gas with 350 V bias voltage, and constant 80 A arc current was applied to the cathodic arc target. Negative bias of −110 V DC was applied to substrate via substrate holder.

2.3 Characterization

The thickness of Ti/ta-C multilayered coating deposited on glass substrate was measured by NanoMap500LS profilometer. FESEM image of the coating was obtained using Carl Zeiss SUPRA 40VP, and elemental analysis was

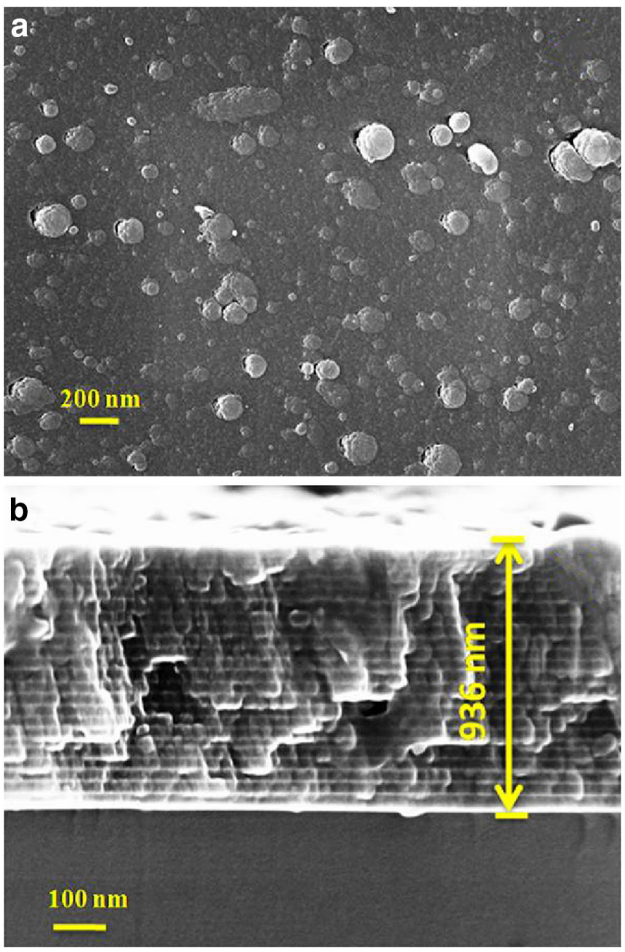

Fig. 1 FESEM images of Ti/ta-C multilayered coating: **a** surface morphology and **b** cross-sectional view of the multilayer

performed by EDS using IncaPentaFETx3 from Oxford Instruments attached to the FESEM. Surface topography was investigated by AFM with CSEM Instruments (Model SSI) operated in contact mode. Raman spectroscopy of the coating was carried out by confocal micro-Raman spectrometer using DILOR-JOBIN-YVON SPEX (LABRAM 010A) with He–Ne laser source having wave length of 632.8 nm. XPS of multilayered coating was recorded with a SPECS spectrometer, Germany, using non-monochromatic AlKα radiation (1486.6 eV) as an X-ray source operated at 150 W (12 kV, 12.5 mA). The binding energies reported here were referenced with C1*s* peak at 284.6 eV. All the individual spectra were recorded with a pass energy and step increment of 40 and 0.05 eV, respectively. For XPS recording, the sample was mounted on a sample holder and placed into a load-lock chamber with an ultrahigh vacuum (UHV) of 8×10^{-8} mbar for 5 h in order to desorb any volatile species present on the surface. After 5 h, the sample was transferred into the analyzing chamber with UHV of 5×10^{-10} mbar and spectra were recorded. Before collecting spectra, surface of the coating was sputtered mildly as oxidized species can be formed on the surface layer in course of deposition process.

2.4 Properties

Nanohardness of the multilayered coating was measured by Nano Hardness Tester (CSM Instruments) with a Berkovich diamond indenter at 1 and 2 mN loads.

Electrochemical studies were performed in 3.5% NaCl solution on bare SS 202 substrate and multilayered Ti-incorporated ta-C samples at 37 ± 1° C. The test was conducted using CH 604 D electrochemical workstation (CH Instruments, USA) and a conventional three-electrode cell consisting of saturated calomel electrode (SCE), Pt and coated and uncoated SS sample as reference, counter and working electrodes, respectively. In order to get steady-state potential, samples were immersed in 3.5% NaCl solution for 1 h and continuously monitored. Electrochemical measurements have resulted in Tafel plot which is represented as log *i* versus potential plot. The corrosion potential (E_{corr}) and corrosion current density (i_{corr}) are obtained from the Tafel plot. The corrosion rates (CR) of substrate and multilayered coating were evaluated using following equation [36, 37]:

$$CR = \frac{K \times i_{corr} \times EW}{\rho} \quad (1)$$

where CR, *K*, i_{corr}, EW and ρ are corrosion rate in mils per year (mpy), constant that defines the unit of the corrosion rate, corrosion current density in A cm^{-2} and density in g cm^{-3}, respectively. The value of *K* is 0.13. The equivalent weight (EW) of SS is 20.43 g eq^{-1}. The density of corroding species which is SS in the present study is 7.9 g cm^{-3}. Electrochemical impedance spectroscopy (EIS) of substrate and coated samples was carried out in 3.5% NaCl solution over a frequency range of 10 mHz to 100 kHz with sinusoidal perturbation potential amplitude of 10 mV on the E_{OCP}. After each experiment, the impedance data were displayed as Bode plots. The Bode plot is a plot of |*Z*| versus *f* and phase angle (θ) versus *f* where |*Z*| and *f* are absolute impedance and frequency, respectively. The acquired data were curve-fitted and analyzed using ZSimpwin program (Princeton Applied Research, USA) to obtain suitable equivalent circuit parameters. The detailed procedure of electrochemical studies and their analyses have been reported elsewhere [38–40].

Wear studies were carried out in a reciprocating-type wear tester (model CM 9084 DuCom) according to ASTM G133-02 standard [41]. However, these tests are not in full compliance with the provisions of Test Method G 133,

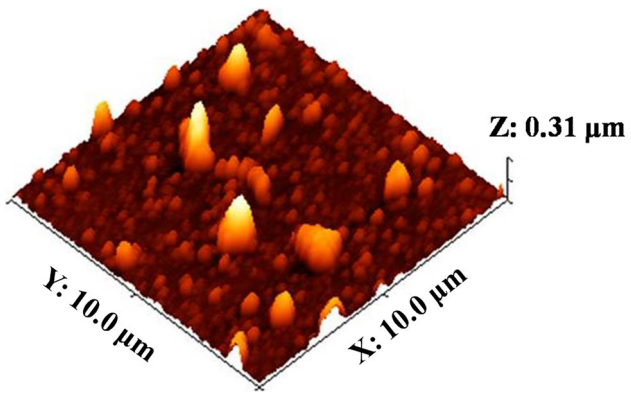

Fig. 2 Surface topography of Ti/ta-C multilayered coating

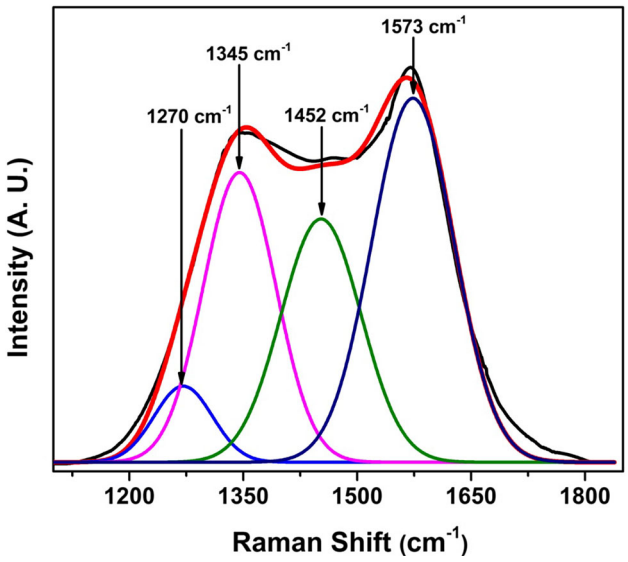

Fig. 3 Raman spectrum of Ti/ta-C multilayered coating

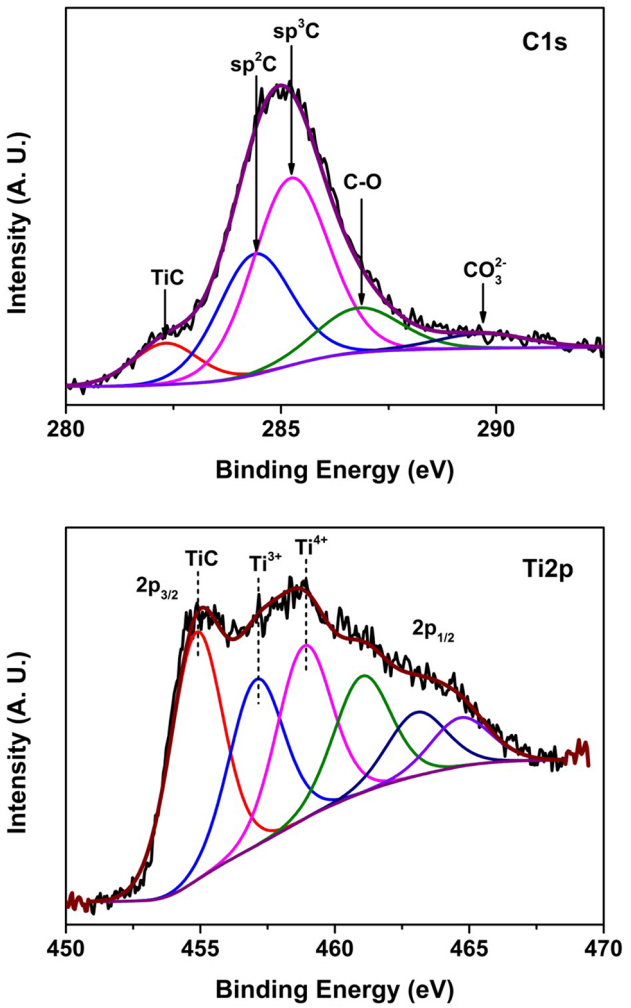

Fig. 4 XPS of C1*s* and Ti2*p* core levels of Ti/ta-C multilayered coating

Procedure A, because the normal forces in these experiments were 2, 5, 7 and 10 N instead of 25 N as prescribed by the standard. Also, the stroke length was 10 mm and an alumina ball of 6 mm diameter was used as the counter surface. Further, the experiments were carried out at a frequency of 100 Hz, and duration of each experiment was 20 min. After the experiments, the samples were examined for wear profile by a profilometer. The wear loss was calculated from the cross-sectional area of the wear profile according to ASTM G133-02 method [41].

3 Results and Discussion

3.1 Thickness, Surface Morphology and Chemical Composition

The thickness of Ti/ta-C multilayered coating has been evaluated from profilometry by masking a small portion of the glass substrate. The obtained total thickness of the coating is 936 nm, and approximate individual thicknesses of the titanium and tetrahedral amorphous carbon layers are less than 10 and ~30 nm, respectively.

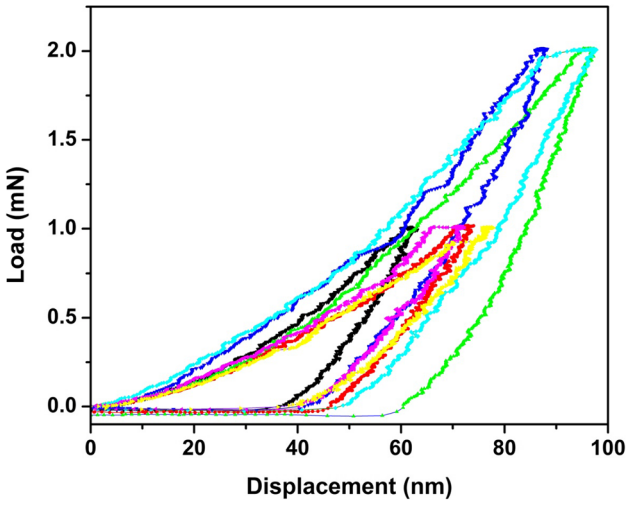

Fig. 5 Load versus displacement curves of Ti/ta-C multilayered coating

Figure 1a shows surface morphology of Ti/ta-C multilayered coating on silicon substrate by FESEM. The non-homogeneous surface is observed over the coating with macrodroplets whose sizes approximately vary from 50 to 220 nm range, and it might be emitted from graphite target during the deposition. Figure 1b displays the typical cross-sectional view of the multilayered Ti-incorporated ta-C coating which consists of dark and thin bright layers corresponding to tetrahedral amorphous carbon and titanium layers.

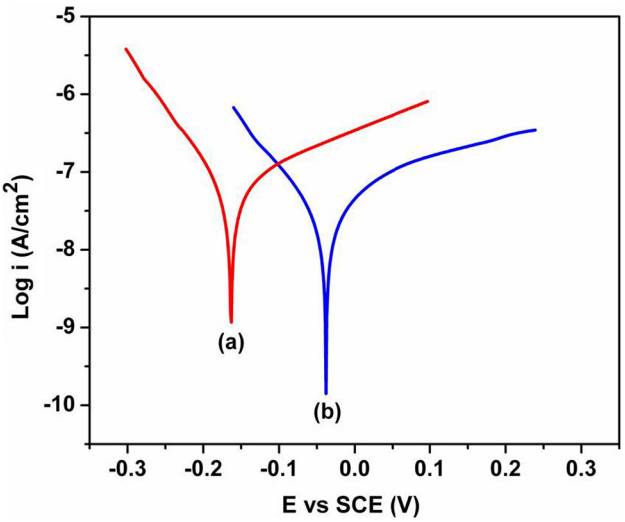

Fig. 6 Potentiodynamic polarization curves for **a** SS 202 substrate and **b** Ti/ta-C multilayered coating samples

The chemical composition of Ti/ta-C multilayered coating has been deduced by EDS. Titanium and carbon concentrations are 9.44 and 90.56 at%, respectively, in the multilayered coating.

3.2 Surface Roughness

The surface topography of the Ti/ta-C multilayered coating is shown in Fig. 2 as three-dimensional (3D) AFM image. The AFM image reveals that coated sample has rough surface with macrodroplets. It has been observed that macrodroplets are not in same size. The average surface roughness (R_a) and root mean square surface roughness (R_q) values have been calculated using the following formulas [42]:

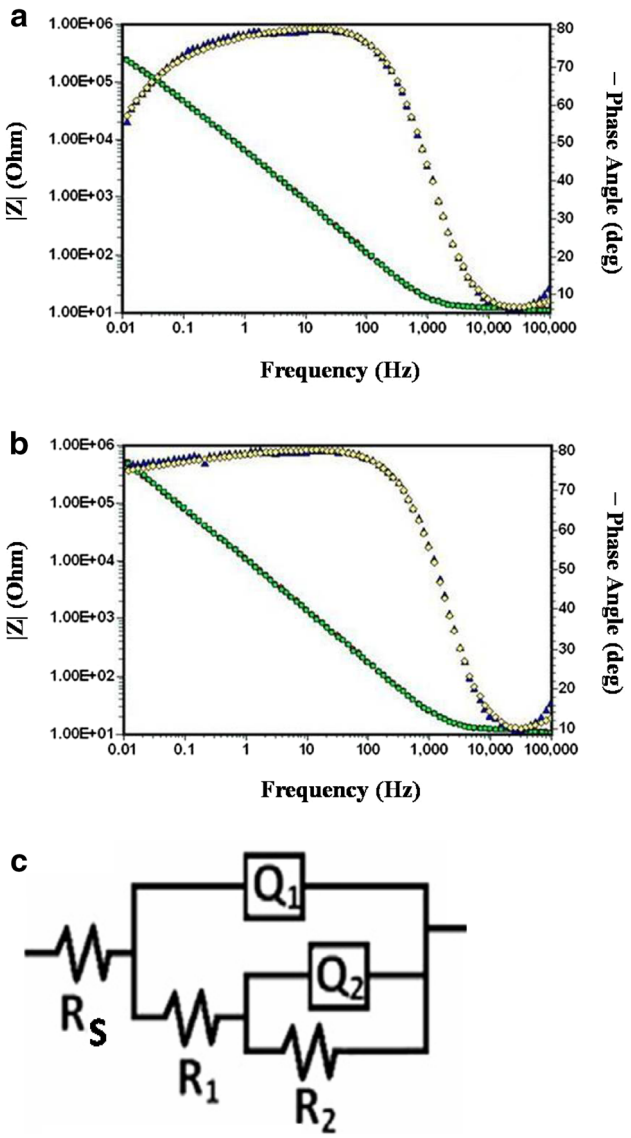

Fig. 7 Bode plots of **a** SS 202 substrate and **b** Ti/ta-C multilayered coating samples, and **c** equivalent circuits (EC)

$$R_a = \frac{1}{L}\int_0^L |Z(x)|\mathrm{d}x \tag{2}$$

$$R_q = \sqrt{\frac{1}{L}\int_0^L |Z(x)|^2\mathrm{d}x} \tag{3}$$

where $Z(x)$ is a function that describes the surface profile analyzed in terms of height (Z) and position (x) of the sample over evaluation length L. The observed average roughness and root mean square roughness values of the multilayered coating are 21 and 36 nm, respectively, over an area of 10.0 × 10.0 μm^2.

3.3 Raman Spectroscopy Studies

Figure 3 shows Raman spectrum of multilayered coating in the range of 900–1800 cm^{-1} range. The broad spectrum of the coating is deconvoluted into four Gaussian peaks in order to get good fit of the DLC coating [43]. The Raman spectrum consists of D and G bands located at 1345 and 1573 cm^{-1}, respectively. The D and G bands are attributed to the bond angle disorder of the sp^2 band and E_{2g} symmetric vibration mode of the sp^2 band [44, 45]. I_D/I_G ratio is significantly used to evaluate the degree of disorder in the carbon network in the coating. However, Li et al. have observed that more layers have lower I_D/I_G value due to less sp^2 sites conversion process at thinner sublayers [46]. In the present work, the I_D/I_G value (obtained from integral areas under the D and G bands) of the coating is approximately 0.51.

3.4 XPS Studies

XPS of Ti/ta-C multilayered coating has been carried out to understand the surface nature of the coating. Oxidation states of constituent elements and concentrations of several component species of respective elements have been evaluated from the XPS that would reflect the characteristics of the coating. Broad and asymmetrical envelopes of C1*s* and Ti2*p* core level spectra of Ti/ta-C multilayer coating indicate the presence of multiple species of carbon and titanium in the coating. Accordingly, they are decomposed into different component species. In Fig. 4, curve-fitted C1*s* and Ti2*p* core level spectra of the multilayered coating are presented. Observed peaks at 282.2, 284.4 and 285.2 eV in the layer correspond to titanium carbide, sp^2C (C=C) and sp^3C (C–C), respectively [39, 47]. Component peaks observed at 286.8 and 289.7 eV are attributed to C–O and CO_3^{2-} species, respectively [48, 49]. Relative amounts of carbidic carbon, sp^2C, sp^3C, C–O and CO_3^{2-} are 8.8, 28.6, 46.1, 12.2 and 4.3%, respectively. Ti2*p* core level spectrum is also resolved into sets of spin–

Table 1 Electrochemical impedance parameters obtained by fitting equivalent circuit model for SS substrate and multilayered Ti/ta-C coated samples

Samples	R_s (Ω cm^2)	Q_1 (S s^n cm^{-2})	N_1	R_1 (Ω cm^2)	Q_2 (S s^n cm^{-2})	N_2	R_2 (Ω cm^2)
SS substrate	6.78	1.19×10^{-5}	0.67	15.67	1.97×10^{-5}	0.94	9.16×10^5
Multilayered Ti/ta-C	11.29	3.24×10^{-5}	0.86	5.88×10^5	1.09×10^{-5}	0.68	8.88×10^7

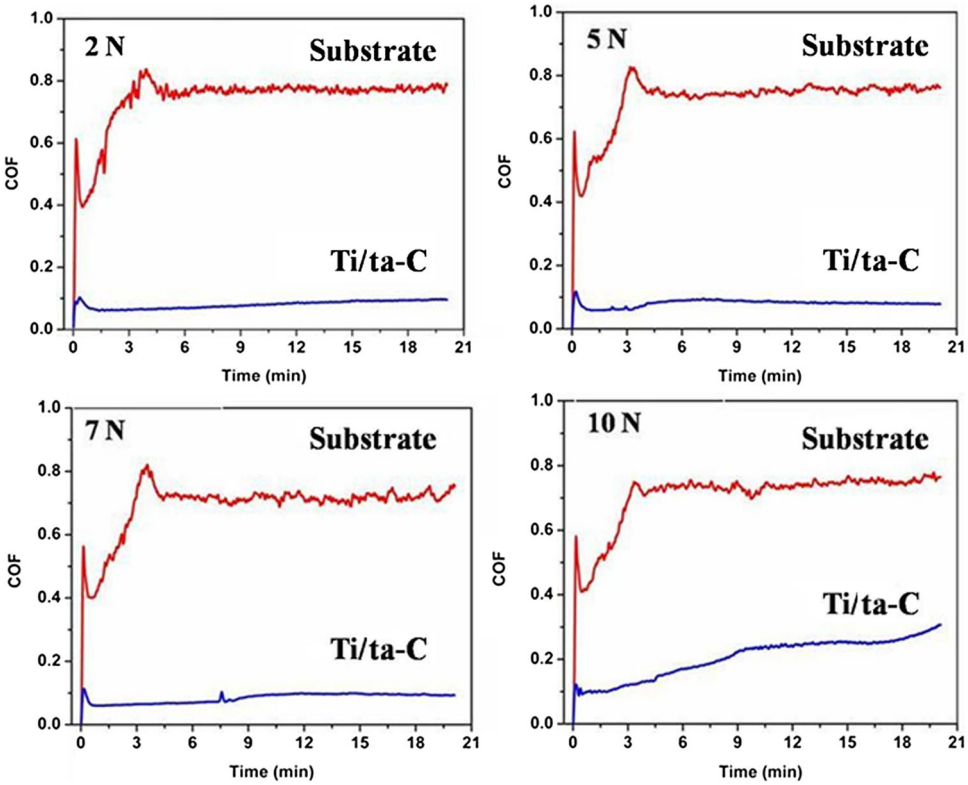

Fig. 8 Coefficient of friction (COF) versus testing time on SS 202 substrate and Ti/ta-C multilayered coating samples at 2, 5, 7 and 10 N loads

orbit doublet peaks. Ti2$p_{3/2,1/2}$ peaks observed at 454.9 and 461.2 eV in the curve-fitted spectrum are assigned for Ti carbide species. Observed doublet peaks at 457.1 and 463.1 and 458.4 and 464.6 eV stand for oxidized Ti^{3+} and Ti^{4+} species, respectively. All these values for Ti carbide, Ti^{3+} and Ti^{4+} species are close to the values reported in the literature [39, 47, 50]. Comparing the intensity of Ti carbide-, Ti^{3+}- and Ti^{4+}-related peaks in the curve-fitted spectrum, it has to be noted that around 41% of total Ti is present as Ti carbide form, 29% of Ti is in Ti^{3+} form, and 30% of Ti is in Ti^{4+} species in Ti/ta-C multilayered coating. Thus, XPS studies demonstrate the presence of Ti carbide and oxidized Ti species and different carbon species in the surface of the multilayered coating.

3.5 Nanoindentation Studies

The mechanical property of the Ti/ta-C multilayered coating is shown in Fig. 5 as a load and displacement curve. The hardness and elastic modulus are evaluated from nanoindentation tests at different places under 1 and 2 mN loads in order to check uniformity of the coating. It has been noticed that due to macrodroplet and non-homogenous surfaces, the hardness and Young's modulus vary place to place. The average hardness at 1 mN load is 15.6 $\pm$ 1.7 and 17 $\pm$ 3.6 GPa for 2 mN load, and values of Young's modulus are 146.8 and 189.1 GPa at 1 and 2 mN loads, respectively. Maximum penetration depth is 97 nm at 2 mN load.

3.6 Corrosion Studies

The corrosion studies have been carried out on SS 202 substrate and Ti/ta-C multilayered coated SS 202 substrate in 3.5% NaCl solution. The potentiodynamic polarization curves of the SS substrate and Ti-incorporated ta-C sample are presented in Fig. 6. The electrochemical parameters, namely corrosion potential (E_{corr}), corrosion current

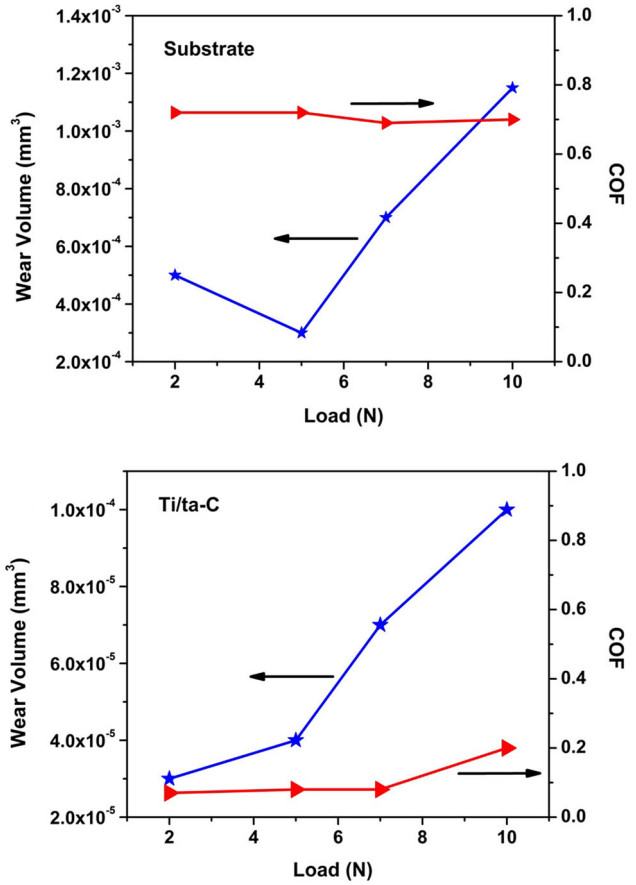

Fig. 9 Plots of COF versus load and wear volume versus load over substrate and Ti/ta-C multilayered coating

density (i_{corr}) and corrosion rate, were obtained for SS 202 substrate and multilayered ta-C coated samples. The corrosion current density (i_{corr}) and corrosion potential (E_{corr}) were deduced from the Tafel plot. The corrosion rates are calculated from Eq. (1). The observed i_{corr} values are 0.05 and 0.02 μA cm^{-2} for SS 202 substrate and multilayered coated sample, respectively. Figure 6 shows that corrosion potential value of multilayered sample is shifted to more positive value of −0.038 V compared to that of −0.163 V for SS 202 substrate. Therefore, Ti/ta-C shows better corrosion resistance characteristics as compared to the uncoated SS 202 substrate. Corrosion rates of SS 202 substrate and multilayered coated substrate sample are 0.017 and 0.007 mpy, respectively. This indicates the enhanced corrosion resistance behavior of the multilayered coating.

Results obtained from EIS with 3.5% NaCl solution are shown in Fig. 7a in the form of Bode plots. For uncoated SS 202 substrate, there is a small change in phase angle occurring from −10° to 0° in the high-frequency range of 10–100 kHz. In the mid-frequency range from 1 to 100 Hz, the phase angle is nearly constant around −80° and decreases to −55° at low-frequency range (0.01–1 Hz), which is less than −90°, the value for an ideal capacitor. In the case of multilayered Ti/ta-C-coated sample in Fig. 7b, the phase angle in the frequency range of 0.1–1000 Hz is −80° and decreases to −75° in the lower-frequency range. However, in order to get EIS parameters, impedance data are fitted with equivalent circuit (EC) diagram. EC is used for understanding the physical process taking place in the system under investigation. Multilayered coated sample and uncoated sample (SS 202) have same two-time-constant equivalent circuit diagram which is presented in Fig. 7c. The EC diagram consists of R_s, R_1 and R_2 representing the solution resistance, outer pores layer resistance and inner layer resistance, respectively. Q_1 represents the capacitance of the outer layer and Q_2 represents the capacitance of the inner layer. The values of the electrical parameters obtained by fitting the impedance data of the substrate and multilayered coating are given in Table 1. The resistance of outer porous layer (R_1) of the substrate is 15.67 Ω cm^2. High corrosion resistance associated with inner oxide layer on the substrate (R_2) is 9.16 × 10^5 Ω cm^2. The value of N for the constant phase element representing the outer layer is 0.67 and that is 0.94 for inner layer. In the case of titanium-incorporated ta-C sample, the outer layer resistance (R_1) is 5.88 × 10^5 Ω cm^2 and inner layer resistance (R_2) is 8.88 × 10^7 Ω cm^2 which are higher than the uncoated SS substrate. Thus, multilayered coating demonstrates good corrosion resistance compared to that of uncoated substrate.

3.7 Wear Studies

The wear behaviors of substrate (SS 202) and Ti/ta-C multilayered coating have been evaluated by reciprocating wear test against with 6 mm Al_2O_3 ball. The wear tests have been carried out at room temperature (relative humidity of 65%) without any lubricant medium. In order to evaluate the coefficient of friction (COF) of the uncoated and coated samples, wear tests have been conducted at different loads such as 2, 5, 7 and 10 N. Figure 8 shows the coefficient of the friction of substrate and coated samples with different applied loads as a function of testing time. Figure 8 shows that, for bare substrate, the friction coefficient possesses stable values of 0.72, 0.72, 0.69 and 0.70 at 2, 5, 7 and 10 N loads, respectively, over time. In the case of Ti/ta-C multilayered coating, the coefficient of friction shows almost constant values of 0.07, 0.08, 0.08 and 0.2 at 2, 5, 7 and 10 N loads, respectively. Figure 9 presents the average coefficient of friction values of bare SS 202 substrate and Ti/ta-C multilayered coating as a function of load.

In order to calculate wear volume of bare substrate and coated samples, 3D and 2D profilometries have been carried out on the wear tracks of 2, 5, 7 and 10 N loads on substrate and Ti/ta-C multilayered coated samples.

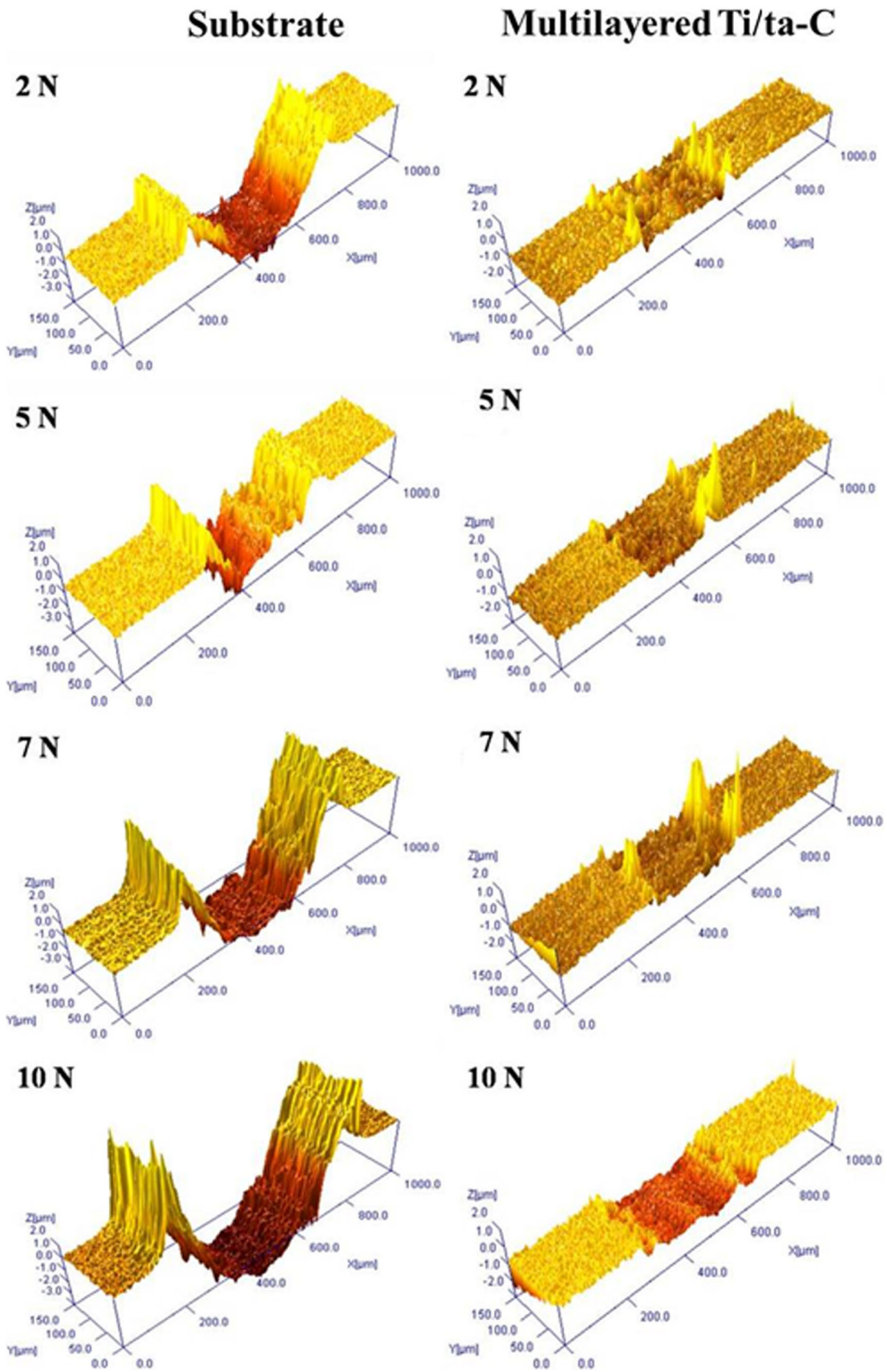
Substrate
Multilayered Ti/ta-C
2 N
2 N
5 N
5 N
7 N
7 N
10 N
10 N
Z[μm]
X[μm]
Y[μm]

◀**Fig. 10** 3D profiles of wear tracks at 2, 5, 7 and 10 N loads on SS 202 substrate and Ti/ta-C multilayered coating samples

Figure 10 shows the 3D images of the wear tracks of substrate and Ti/ta-C multilayered coating. It can be seen from the figures that the wear profiles on the substrate have deep grooves while the wear tracks on the Ti/ta-C multilayered coated samples have less deep. The average wear volumes calculated from wear profiles of substrate and multilayered coating are also shown in Fig. 9. In the case of substrate, the wear volumes are 0.0005, 0.0003, 0.0007 and 0.00115 mm^3 at 2, 5, 7 and 10 N loads, respectively. However, in the case of Ti/ta-C multilayered coating, the wear volumes are 0.00003, 0.00004, 0.00007 and 0.00010 mm^3 at 2, 5, 7 and 10 N loads, respectively. Compared to uncoated substrate, Ti/ta-C multilayered coated sample shows very low COF values as well as wear volumes and wear marks are also shallower. Thus, Ti/ta-C multilayered coating reduces the wear volumes.

4 Conclusions

Ti/ta-C multilayered coating has been deposited by combination of magnetron sputtering and cathodic arc evaporation alternatively on silicon, glass and stainless steel (SS 202) substrates. Obtained coating thickness is $\sim$936 nm. Raman spectroscopy studies show the features of DLC coating. XPS studies show the presence of titanium carbide species in the coating along with oxidized species. Average hardness values of 15.6 $\pm$ 1.7 and 17 $\pm$ 3.6 GPa at 1 and 2 mN loads are obtained in the coating. The electrochemical studies demonstrate that the Ti/ta-C multilayered coating exhibits better corrosion resistance compared to that of the SS 202 substrate. Wear studies show that Ti/ta-C multilayered coated substrate has very low coefficient of friction and low wear volumes at 2, 5, 7 and 10 N loads studied in the present work.

Acknowledgements The work was carried out under the CSIR network project ESC-01-01. The authors would like to thank the Director, CSIR-National Aerospace Laboratories, Bengaluru, for his support and permission to publish the work and also thank Mr. Siju John, Mr. V. Praveen Kumar, Ms. Latha and Mr. Muniprakash for FESEM, AFM, 3D, 2D profilometry, Raman spectroscopy and wear studies, respectively.

Compliance with Ethical Standards

Conflict of interest On behalf of all authors, the corresponding author states that there is no conflict of interest regarding this paper.

References

1. Robertson J (1991) Hard amorphous (diamond-like) carbons. Prog Solid State Chem 21:199–333
2. Robertson J (1992) Properties of diamond-like carbon. Surf Coat Technol 50:185–203
3. Fallon PJ, Veerasamy VS, Davis CA, Robertson J, Amaratunga GAJ, Milne WI, Koskinen J (1993) Properties of filtered-ion-beam-deposited diamond like carbon as a function of ion energy. Phys Rev B 48:4777–4782
4. Lifshitz Y (1996) Hydrogen-free amorphous carbon films: correlation between growth conditions and properties. Diamond Relat Mater 5:388–400
5. McKenzie DR (1996) Tetrahedral bonding in amorphous carbon. Rep Prog Phys 59:1611–1664
6. McKenzie DR, Muller D, Pailthorpe BA, Wang ZH, Kravtchinskaia E, Segal D, Gaskell PH (1991) Properties of tetrahedral amorphous carbon prepared by vacuum arc deposition. Diamond Relat Mater 1:51–59
7. Veerasamy VS, Amaratunga GAJ, Milne WI, Hewitt P, Fallon PJ, McKenzie DR, Davis CA (1993) Optical and electronic properties of amorphous diamond. Diamond Relat Mater 2:782–787
8. Satyanarayana BS, Hart A, Milne WI, Robertson J (1998) Field emission from tetrahedral amorphous carbon. Diamond Relat Mater 7:656–659
9. Aksenov II, Vakula SI, Padalka VG, Strelnitskii VE, Khoroshikh VM (1980) High-efficiency source of pure carbon plasma. Zh Tekh Fiz 50:2000–2004
10. Coll BF, Chhowalla M (1996) Amorphous diamond film by enhanced arc deposition. Surf Coat Technol 79:76–86
11. Boxman RL, Zhitomirsky V, Alterkop B, Gidalevich E, Beilis I, Keidar M, Goldsmith S (1996) Recent progress in filtered vacuum arc deposition. Surf Coat Technol 86:243–253
12. Polo MC, Andujar JL, Hart A, Robertson J, Milne WI (2000) Preparation of tetrahedral amorphous carbon films by filtered cathodic vacuum arc deposition. Diamond Relat Mater 9:663–667
13. Inaba H, Furusawa K, Hirano S, Sasaki S, Todoroki S, Yamasaka M, Endou M (2003) Tetrahedral amorphous carbon films by filtered cathodic vacuum-arc deposition for air-bearing-surface overcoat. Jpn J Appl Phys 42:2824–2828
14. Kok YN, Hovsepian PE, Luo Q, Lewis DB, Wen JG, Petrov I (2005) Influence of the bias voltage on the structure and the tribological performance of nanoscale multilayer C/Cr PVD coatings. Thin Solid Films 475:219–226
15. Yi P, Peng L, Zhou T, Wu H, Lai X (2013) Development and characterization of multilayered Cr–C/aC: Cr film on 316L stainless steel as bipolar plates for proton exchange membrane fuel cells. J Power Sources 230:25–31
16. Chang YY, Wang DY, Wu W (2002) Catalysis effect of metal doping on wear properties of diamond-like carbon films deposited by a cathodic-arc activated deposition process. Thin Solid Films 420:241–247
17. Lin YH, Lin HD, Liu CK, Huang MW, Chen YC, Chen JR, Shih HC (2009) Annealing effect on the structural, mechanical and electrical properties of titanium-doped diamond-like carbon films. Thin Solid Films 518:1503–1507
18. Kulikovsky VY, Fendrych F, Jastrabik L, Chvostova D (1997) Study of formation and some properties of Ti–C: H films prepared by dc magnetron sputtering. Surf Coat Technol 91:122–130
19. Singer IL (1992) Solid lubrication processes. In: Singer IL, Pollock HM (eds) Fundamentals of friction: macroscopic and microscopic processes. Springer, Dordrecht, pp 237–261
20. Zhao F, Li H, Ji L, Wang Y, Zhou H, Chen J (2010) Ti-DLC films with superior friction performance. Diamond Relat Mater 19:342–349
21. Cui J, Qiang L, Zhang B, Ling X, Yang T, Zhang J (2012) Mechanical and tribological properties of Ti-DLC films with different Ti content by magnetron sputtering technique. Appl Surf Sci 258:5025–5030

22. Qiang L, Zhang B, Zhou Y, Zhang J (2013) Improving the internal stress and wear resistance of DLC film by low content Ti doping. Solid State Sci 20:17–22
23. Ziegele H, Scheibe HJ, Schultrich B (1997) DLC and metallic nanometer multilayers deposited by laser-arc. Surf Coat Technol 97:385–390
24. Bootkul D, Saenphinit N, Supsermpol B, Aramwit C, Intarasiri S (2014) Synthesis of Ti-doped DLC film on SS304 steels by filtered cathodic vacuum arc (FCVA) technique for tribological improvement. Appl Surf Sci 310:293–299
25. Lin YH, Lin HD, Liu CK, Huang MW, Chen JR, Shih HC (2010) Structure and characterization of the multilayered Ti-DLC films by FCVA. Diamond Relat Mater 19:1034–1039
26. Weng KW, Chen YC, Lin TN, Wang DY (2006) Metal-doped diamond-like carbon films synthesized by filter-arc deposition. Thin Solid Films 515:1053–1057
27. Anttila A, Salo J, Lappalaimen R (1995) High adhesion of diamond-like films achieved by pulsed arc-discharge method. Mater Lett 24:153–156
28. Wu WY, Ting JM (2006) Growth and characteristics of metal-containing diamond-like carbon using a self-assembled process. Carbon 44:1210–1217
29. Meng WJ, Curtis TJ, Rehn LE, Baldo PM (1998) Plasma-assisted deposition and characterization of Ti-containing diamond like carbon coatings. J Appl Phys 83:6076–6081
30. Wu WJ, Hon MH (1999) Thermal stability of diamond-like carbon films with added silicon. Surf Coat Technol 111:134–140
31. Cho YK, Jang WS, Yoo S, Kim SG, Kim SW (2008) Synthesis of conductive Ti–C: H films on the stainless steel plates by PECVD process. Surf Coat Technol 202:5390–5394
32. Weng KW, Chang CL, Wang DY (2002) Effect of ion energy on degradation of diamond-like carbon films exposed to high-energy bombardment from an ion implanter. Diamond Relat Mater 11:1447–1453
33. Byon E, Kim JK, Rha JJ, Kwon SC, Mu Z, Liu C, Li G (2007) Effect of metal ion implantation on thermal instability of diamond-like carbon films. Surf Coat Technol 201:6670–6673
34. Cui L, Guoqing L, Wenwu C, Zongxin M, Chengwu Z, Liang W (2005) The study of doped DLC films by Ti ion implantation. Thin Solid Films 475:279–282
35. Baba K, Hatada R (2003) Deposition and characterization of Ti- and W-containing diamond-like carbon films by plasma source ion implantation. Surf Coat Technol 169:287–290
36. ASTM G102-89 (1999) Standard practice for calculation of corrosion rates and related information from electrochemical measurements
37. Lakshmi RV, Yoganandan G, Kavya KT, Basu BJ (2013) Effective corrosion inhibition performance of Ce^{3+} doped sol-gel nanocomposite coating on aluminium alloy. Prog Org Coat 76:367–374
38. Stern M, Geary AL (1957) Electrochemical polarization I: a theoretical analysis of the shape of polarization curves. J Electrochem Soc 104:56–63
39. Mohan L, Anandan C, Grips VW (2012) Corrosion behavior of titanium alloy Beta-21S coated with diamond like carbon in Hank's solution. Appl Surf Sci 258:6331–6340
40. Mohan L, Anandan C (2013) Wear and corrosion behavior of oxygen implanted biomedical titanium alloy Ti–13Nb–13Zr. Appl Surf Sci 282:281–290
41. Kumar P, Babu PD, Mohan L, Anandan C, Grips VW (2013) Wear and corrosion behavior of Zr-doped DLC on Ti–13Zr–13Nb biomedical alloy. J Mater Eng Perform 22:283–293
42. De Oliveira RRL, Albuquerque DAC, Cruz TG, Yamaji FM, Leite FL (2012) Measurement of nanoscale roughness by atomic force microscopy: basic principles and applications. In: Bellitto V (ed) Atomic force microscopy: imaging, measuring and manipulating surfaces at the atomic scale. In Tech, Rijeka
43. Tai FC, Lee SC, Chen J, Wei C, Chang SH (2009) Multipeak fitting analysis of Raman spectra on DLCH film. J Raman Spectrosc 40:1055–1059
44. Richter A, Scheibe HJ, Pompe W, Brzezinka KW, Mühling I (1986) About the structure and bonding of laser generated carbon films by Raman and electron energy loss spectroscopy. J Non-Cryst Solids 88:131–144
45. Lin YH, Lin HD, Liu CK, Huang MW, Chen YC, Chen JR, Shih HC (2009) Annealing effect on the structural, mechanical and electrical properties of titanium-doped diamond-like carbon films. Thin Solid Films 518:1503–1507
46. Li F, Zhang S, Kong J, Zhang Y, Zhang W (2011) Multilayer DLC coatings via alternating bias during magnetron sputtering. Thin Solid Films 519:4910–4916
47. Zhang S, Fu YQ, Bui XL, Du HJ (2004) XPS study of diamond-like carbon-based nanocomposite films. Int J Nanosci 3:797–802
48. Santra S, Ranjan P, Bera P, Ghosh P, Mandal SK (2012) Anchored palladium nanoparticles onto single walled carbon nanotubes: efficient recyclable catalyst for N-containing heterocycles. RSC Adv 2:7523–7533
49. Younesi R, Norby P, Vegge T (2014) A new look at the stability of dimethyl sulfoxide and acetonitrile in Li–O_2 batteries. ECS Electrochem Lett 3:A15–A18
50. Navas J, Sánchez-Coronilla A, Aguilar T, Hernández NC, de los Santos DM, Sánchez-Márquez J, Zorrilla D, Fernández-Lorenzo C, Alcántara R, Martín-Calleja J (2014) Experimental and theoretical study of the electronic properties of Cu-doped anatase TiO_2. Phys Chem Chem Phys 16:3835–3845